Cell Host & Microbe
Article

Aldolase Is Essential for Energy Production and Bridging Adhesin-Actin Cytoskeletal Interactions during Parasite Invasion of Host Cells

G. Lucas Starnes,[1] Mathieu Coincon,[2] Jurgen Sygusch,[2] and L. David Sibley[1,*]
[1]Department of Molecular Microbiology, Washington University School of Medicine, 660 S. Euclid Avenue, St. Louis, MO 63130-1093, USA
[2]Department of Biochemistry, 2900 Boulevard Edouard-Montpetit, University of Montreal, Montreal, Quebec H3T 1J4, Canada
*Correspondence: sibley@borcim.wustl.edu
DOI 10.1016/j.chom.2009.03.005

SUMMARY

Apicomplexan parasites rely on actin-based motility to drive host cell invasion. Prior in vitro studies implicated aldolase, a tetrameric glycolytic enzyme, in coupling actin filaments to the parasite's surface adhesin microneme protein 2 (MIC2). Here, we test the essentiality of this interaction in host cell invasion. Based on in vitro studies and homology modeling, we generated a series of mutations in *Toxoplasma gondii* aldolase (*TgALD1*) that delineated MIC2 tail domain (MIC2t) binding function from its enzyme activity. We tested these mutants by complementing a conditional knockout of *TgALD1*. Mutations that affected glycolysis also reduced motility. Mutants only affecting binding to MIC2t had no motility phenotype, but were decreased in their efficiency of host cell invasion. Our studies demonstrate that aldolase is not only required for energy production but is also essential for efficient host cell invasion, based on its ability to bridge adhesin-cytoskeleton interactions in the parasite.

INTRODUCTION

Toxoplasma gondii causes opportunistic infections in immunocompromised patients and the developing fetus (Hill and Dubey, 2002). As an obligate intracellular pathogen, *T. gondii* must penetrate host cells to replicate and survive, a process shared by related apicomplexans such as malaria (*Plasmodium* spp.) (Sibley, 2004). Host cell invasion is based on gliding motility, a substrate-dependent mode of locomotion unique to these organisms and an essential component of parasite dissemination (Sibley, 2004). Gliding motility relies on formation of actin filaments, and their chemical disruption renders the parasite immotile (Wetzel et al., 2003) and also prevents host cell invasion (Dobrowolski and Sibley, 1996). Motility also relies on TgMyoA, a class XIV myosin that provides the motive force (Meissner et al., 2002). TgMyoA, with its regulatory light chain (TgMLC1), is anchored into the inner membrane complex through association with the integral membrane protein TgGAP50 (Gaskins et al., 2004; Opitz and Soldati, 2002). Thus anchored, the nonprocessive motor walks along actin filaments toward the barbed end, while contact with the substratum is provided by micronemal proteins that are deposited at the parasite apex following secretion (Sibley, 2004).

One important group of micronemal proteins that contributes to motility and invasion is the thrombospondin-related anonymous protein (TRAP) family (Robson et al., 1995). Originally identified in *P. falciparum*, paralogues were subsequently identified in other motile stages of the malarial life cycle (Dessens et al., 1999; Yuda et al., 1999) and orthologs in other apicomplexans, such as *Eimeria* and *Cryptosporidium* (Spano et al., 1998; Tomley et al., 1991). TRAP is essential in gliding motility and invasion of the mosquito salivary glands by *P. berghei* sporozoites (Sultan et al., 1997). The TRAP ortholog in *T. gondii* is known as MIC2 (Wan et al., 1997), which is also essential to parasite motility, adherence, and efficient host cell invasion (Huynh and Carruthers, 2006). Like other TRAP proteins, MIC2 contains extracellular domains related to integrin A domain and thrombospondin type 1 (TSR1) repeats, a transmembrane region, and a short cytoplasmic domain (Wan et al., 1997). The extracellular A domains are thought to bind receptors on host cells or substratum, including glycosaminoglycans and heparin-like molecules, thus providing anchorage for traction (Harper et al., 2004; Ménard, 2001). The cytoplasmic tails of MIC2 (MIC2t) and TRAP (TRAPt) were found to interact in vitro with the glycolytic enzyme aldolase (Buscaglia et al., 2003; Jewett and Sibley, 2003). This interaction depends upon a conserved penultimate tryptophan and a collection of acidic residues at the C terminus of the cytoplasmic domain (Buscaglia et al., 2003; Starnes et al., 2006). The generation of a cocrystal structure of aldolase with a TRAPt peptide highlighted the importance of the conserved penultimate tryptophan and surrounding acidic residues, which are believed to establish a series of hydrogen bonds with charged residues near the enzyme active site (Bosch et al., 2007). Based on these in vitro studies, it was proposed that aldolase may serve as the bridge between the adhesin and the cytoskeleton in vivo, thereby connecting external adhesins to the actin-myosin motor (Jewett and Sibley, 2003).

In eukaryotes, class I aldolase exists as a homotetrameric enzyme (Penhoet et al., 1967) that participates in glycolysis by cleaving fructose-1,6-bisphosphate into two products: glyceraldehyde-3-phosphate and dihydroxy-acetone phosphate (Meyerhof et al., 1936). Each subunit of aldolase contains an active site, situated in the center of the established $(\alpha/\beta)_8$ barrel fold (Sygusch et al., 1987). The tetrameric state of the enzyme provides a platform for aldolase to crosslink actin filaments

through a conserved set of residues that overlaps the catalytic pocket (Wang et al., 1996). The ability of aldolase to bind both F-actin and the cytoplasmic tails of adhesins such as MIC2 (MIC2t) and TRAP (TRAPt) may facilitate bridging of the adhesin to the cytoskeleton during gliding motility in apicomplexans. Despite compelling in vitro data supporting aldolase-MIC2t interactions and evidence for colocalization and coprecipitation from parasite lysates (Buscaglia et al., 2003; Jewett and Sibley, 2003), the essentiality of this interaction in vivo remains untested. Moreover, this model predicts that aldolase separately participates in glycolysis and bridges to the actin cytoskeleton, raising the issue of how these disparate activities are controlled.

In the current study, we sought to directly test the role of aldolase in bridging adhesin-cytoskeletal interactions during motility and invasion in the parasite. To this end, we generated a series of aldolase mutations that delineated MIC2t binding from enzyme activity and tested these by complementing a conditional knockout (cKO) of *T. gondii* aldolase (*TgALD1*).

RESULTS

Homology Modeling and Mutational Analysis of TgALD1

Previous studies demonstrated that a stretch of acidic residues in MIC2t that flank a tryptophan residue (MIC2-W767) are critical for binding to TgALD1 in vitro (Figure S1) (Starnes et al., 2006). Homology modeling of TgALD1 revealed a basic groove that surrounds the substrate-binding pocket (Figure S1). Residues previously implicated in F-actin binding were also encompassed in this same basic cleft (Figure S1) (Wang et al., 1996). The basic nature of this cleft suggested it may interact with the acidic MIC2t through electrostatic interactions. Modeling the interaction with aldolase revealed that the indole ring of MIC2-W767 was sandwiched between the hydrophobic side chains of aldolase arginine 303 (ALD-R303) and aldolase arginine 42 (ALD-R42), while the carboxyl group of MIC2-D765 makes several key hydrogen bonds with basic side groups in ALD-R148, ALD-K41, and ALD-R42 (Figure 1A). These modeling experiments predict the importance of both electrostatic and hydrophobic interactions in mediating the binding of the MIC2t to TgALD1.

To determine if the basic cleft of aldolase contributes to the interaction with the MIC2t, we generated a series of alanine point mutants in TgALD1. The ability of these TgALD1 mutants to bind to a GST-MIC2t fusion protein was assessed using an in vitro pull-down assay. Residues within the basic cleft of TgALD1 were found to contribute to the interaction with the MIC2t (Figure 1B). Mutations ALD-K146A and ALD-R148A demonstrated the greatest decreases in binding (Figure 1C and Table 1), while the mutations ALD-K41A, ALD-R42A, and ALD-K106A showed partial reductions compared to the wild-type enzyme (Figure 1C and Table 1). The double mutant ALD-K41E, R42G exhibited a loss in binding nearly equal to the single mutant ALD-R148A. Other mutations had modest to no effects, except ALD-E34A, which showed a 2-fold increase in binding. Collectively, these results demonstrate that the MIC2t interacts with key residues in the basic groove of aldolase, with the most significant contributions residing deep within the pocket and along a positively charged ridge defined by K41 and R42.

Since residues implicated in binding to the MIC2t were close to the substrate-binding site, the same point mutants were also evaluated for enzyme activity. Most mutants that exhibited decreased binding also showed defects in enzyme activity (Table 1). In contrast, ALD-K41A and ALD-R42A retained levels similar to wild-type enzyme activity, as shown by k_{cat} levels. While the double mutant ALD-K41E, R42G retained partial activity, it showed a 5-fold reduction in k_{cat}. Collectively, the aldolase mutations were assigned to one of three classes (Figure 1D and Table 1). The first class includes those residues that have minimal decrease in the interaction with the MIC2t but cannot cleave substrate (orange in Figure 1D, typified by ALD-D33A, and Table 1). The second and largest group was unable to carry out either function (blue in Figure 1D, typified by ALD-R148A, and Table 1). The final class of mutations, including ALD-K41A, ALD-R42A, and the double mutant ALD-K41E, R42G, retained normal or partial enzyme activity but had significant decreases in MIC2t binding (green in Figure 1D and Table 1). Collectively, these results demonstrate an overlap between the enzyme active site and the MIC2t binding surfaces, yet also indicate that the two functional interfaces can be separated by specific mutations.

The bridging model predicts that aldolase also interacts with F-actin in order to connect the cytoplasmic tails of adhesins with the cytoskeleton, thus assuring force transduction. Representatives from each of the above classes of aldolase mutations were evaluated for F-actin binding in a cosedimentation assay. Approximately 55% of the wild-type enzyme was associated with F-actin, while the ALD-D33A mutation demonstrated a 2-fold decrease in binding. All other mutations examined exhibited an approximately 5-fold decrease in their binding capacity (Figures 1E and 1F). These results imply that the aldolase surfaces responsible for binding to F-actin and MIC2t largely overlap.

Localization of TgALD1 during Intracellular Growth and Extracellular Motility

Previous studies using heterologous antisera to rabbit aldolase indicated that TgALD1 was apically localized and deposited in the trails of gliding parasites (Jewett and Sibley, 2003). However, this finding has been recently questioned by a study reporting that aldolase, along with other components of glycolysis, are translocated to the periphery in extracellular versus intracellular *T. gondii* parasites (Pomel et al., 2008). To further evaluate the location of aldolase, a polyclonal antisera raised against TgALD1 was used to visualize aldolase during intracellular growth and extracellular gliding. In parasites growing intracellularly, aldolase was localized to the cytoplasm and demonstrated a partial apical colocalization with MIC2, consistent with previous reports (Jewett and Sibley, 2003). A second cytoplasmic protein, pyruvate kinase (PK), exhibited a similar cytoplasmic localization but without a concentration at the apical end (Figure 2). During gliding motility, aldolase remained primarily cytoplasmic in a pattern that was concentrated at the apical end, with a small amount being deposited in the trails (Figure 2B, arrowheads). Quantification of these distributions using a profile plot along the anterior-posterior axis confirmed that aldolase shows a strong apical to posterior gradient, unlike PK that was uniformly distributed (Figure 2B). When the profile was drawn perpendicular to the long axis, aldolase was not concentrated appreciably at the cell periphery, but instead was consistently elevated throughout the cytosol, resulting in a plateau effect (Figure 2B). In parasites

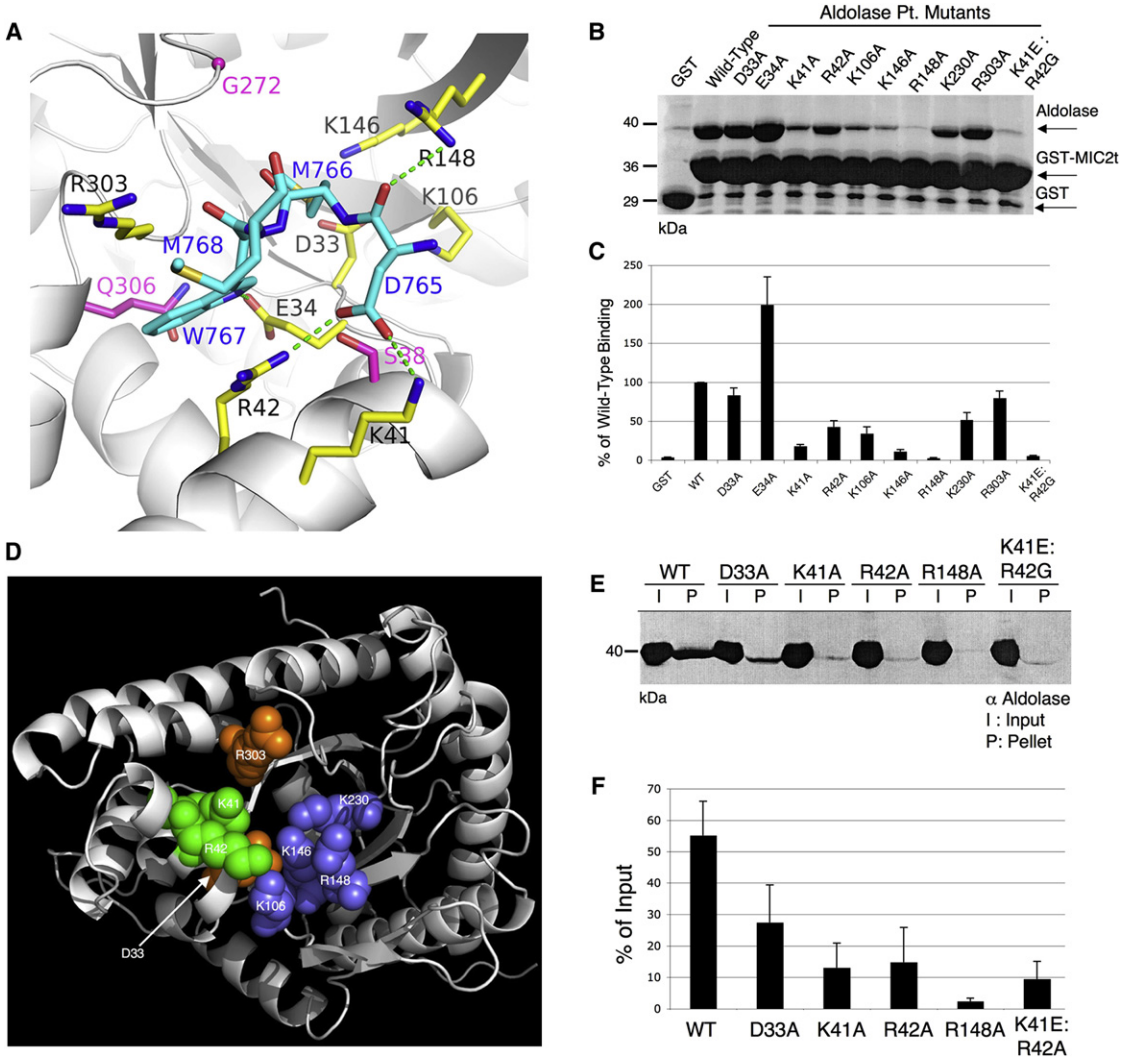

Figure 1. Homology Modeling and Mutational Analysis of the MIC2 Tail Interaction with Aldolase

(A) MIC2t peptide (green) modeled in the TgALD1 basic cleft showing residues within 4 Å and potential electrostatic interactions and hydrogen bonds (green lines).

(B) Binding of wild-type and aldolase mutants to GST-MIC2t by pull-down, resolved by SDS-PAGE and stained with SYPRO Ruby. kDa, molecular mass.

(C) Quantification of three independent experiments from (B); values normalized to wild-type (WT) and graphed as means ± SEM.

(D) *T. gondii* aldolase model depicting key residues as space filling Van Der Waal's spheres. When mutated to Ala, residues in orange (D33, E34, and R303) bound to MIC2t but were enzymatically inactive; residues in blue (K106, K146, R148, and K230) were incapable of either activity, while the residues in green (K41 and R42) had reduced binding to MIC2t, but retained wild-type levels of enzyme activity.

(E) Binding of representative aldolase mutants to F-actin by cosedimentation; pellet (P) versus input (I) detected by western blot using rabbit anti-*T. gondii* aldolase antisera.

(F) Histogram quantification of three independent experiments of (E), mean ± SEM.

that were undergoing gliding, aldolase, as well as the surface protein SAG1, was deposited in trails (Figure 2B, bottom panel). These results support our previous conclusion that aldolase was found in the cytosol, concentrated at the anterior end of the parasite, and deposited in the trails during gliding motility (Jewett and Sibley, 2003) and are similar to reports of the distribution of aldolase in malaria sporozoites (Buscaglia et al., 2003).

Complementation of a *TgALD1* Conditional Knockout

To test the role of aldolase in vivo, we utilized the tetracycline (Tet)-repressible system to generate a cKO (Meissner et al., 2002). The genome of *T. gondii* contains two genes that are annotated as fructose-1,6-bisphosphate aldolase, although only one of these is expressed in tachyzoites at the mRNA level (G.L.S. and L.D.S., unpublished data), as reported previously (Pomel et al., 2008). The functional *TgALD1* locus was disrupted by homologous recombination in a merodiploid line expressing a regulatable, HA-9-epitope-tagged copy of *TgALD1* (Figure 3A). Multiple cKO clones exhibited equivalent levels of downregulation, and from this pool a single clone was selected for further analysis. The cKO parasites were initially characterized by immunofluorescence, using the anti-TgALD1 antibody following

Table 1. Biochemical Characterization of *T. gondii* Aldolase Point Mutations

Mutation	MIC2t Binding[a]	Enzyme Activity (K_{cat})[b]	Actin Binding[c]	Cellular [ATP] (nM)[d]
Wild-Type	100%	141.9 ± 3.9	55% ± 10.8%	254.8 ± 3.4
D33A	83% ± 9.4%	NDA	27% ± 11.9%	135.7 ± 1.3
E34A	199% ± 36.0%	14.2 ± 4.8	NT	NT
K41A	18% ± 2.0%	157.9 ± 18.9	13% ± 7.9%	256.0 ± 4.7
K41E	25%	140.2 ± 16.4	NT	NT
R42A	43% ± 8.0%	131.8 ± 30.7	14% ± 11.0%	223.1 ± 3.4
R42D	25%	NDA	NT	NT
K41A:R42A	75%	NDA	NT	NT
K41E:R42G	5% ± 0.7%	21.2 ± 20.6	9% ± 5.6%	319.2 ± 26.5
K106A	34% ± 8.6%	NDA	NT	NT
K146A	11% ± 2.5%	NDA	NT	NT
R148A	2% ± 0.3%	NDA	2% ± 1.0%	120.0 ± 7.6
K230A	51% ± 9.2%	NDA	NT	NT
R303A	80% ± 8.9%	0.31 ± 3.2	NT	NT
Q306F	3.50%	NDA	NT	NT
Q306G	95%	171.8 ± 4.7	NT	NT

NDA, no detectable activity; NT, not tested.
[a] Average percent binding as determined by triplicate SYPRO Ruby-stained gels, expressed as percent of wild-type (±SEM, n = 3 or mean).
[b] Average of three independent experiments (±SEM).
[c] Percent binding determined as average of triplicate F-actin:aldolase cosedimentation assays by quantitative western blot (±SEM).
[d] Representative experiment comparing stably expressed transgenes in the cKO background and tested in the presence of ATc (n = 3, mean ± SD).

growth for 24 hr in the presence of 1.5 μg/ml anhydrotetracycline (ATc) (Figure 3B). cKO parasites expressed slightly less aldolase than the parental TATi-1 line in the absence of ATc, but importantly, expression was strongly reduced when cultured in ATc. Downregulation of aldolase was determined by quantitative western blot following growth in 1.5 μg/ml ATc and found to be decreased by ~95% (Figure 3C). As expected, the presence of ATc had no effect on TgALD1 levels in the TATi-1 line. These experiments demonstrate successful disruption of the chromosomal copy of *TgALD1* and significant downregulation of the Tet-regulatable copy of *TgALD1* in the cKO.

To test the aldolase-bridging model in vivo, it was paramount to differentiate between parasites compromised in glycolysis versus those with selective disruption of the motor complex. To independently address these functions, a wild-type, c-Myc-epitope-tagged *TgALD1* and a representative from each class of aldolase mutation described above were used to complement the cKO. Approximately equal levels of protein expression were determined by western blot analysis (Figure 4A), with the exception of the double mutant ALD-K41E, R42G, which showed elevated levels. Proper cytoplasmic localization was confirmed by immunofluoresence against the c-Myc epitope (Figure 4B). The resulting complemented parasite clones were used to test the role of aldolase in bridging MIC2t to the actin cytoskeleton versus its contribution to glycolysis.

Evaluation of Parasite Growth and ATP Production

The contribution of aldolase to parasite survival was initially evaluated using a monolayer lysis assay, which captures invasion, replication, egress, and reinvasion of a host cell monolayer. Addition of ATc prevented the cKO and lines complemented with the enzyme null mutants (i.e., ALD-D33A and ALD-R148A) from disrupting the monolayer (Figure 5A), reflecting decreased growth of these lines. In contrast, complementation with mutants having normal enzyme activity (i.e., ALD-K41A and ALD-R42A) led to disruption of the monolayer, even in the presence of ATc (Figure 5A), except for the double mutant ALD-K41E, R42G, which showed a partial reduction in host cell monolayer lysis (Figure 5A). In the absence of ATc, the cKO and all of the complemented clones were able to lyse the host monolayer efficiently, thus demonstrating that none of the constructs exerted a dominant negative phenotype (Figure 5A).

To determine the contribution of aldolase to parasite replication, the average number of parasites per parasitophorous vacuole was determined by microscopic examination. Following culture in ATc, the cKO demonstrated a significant growth defect compared to the absence of ATc (Figure 5B). In agreement with the lytic assay, the cKO complemented with wild-type aldolase and the mutants that retained enzyme activity rescued the growth defect in the presence of ATc, while those without detectable enzyme activity did not (Figure 5B). In contrast to the lytic assay, the double mutant ALD-K41E, R42G grew normally in the presence of ATc, indicating that it was capable of supporting normal parasite replication. The appreciated growth defects were a direct result of the presence of ATc, as all parasite lines grew equally well in its absence (data not shown).

In addition, we determined cellular ATP concentrations using a luciferase assay. Comparison of the cKO in the absence ([ATP] $\geq$ 236 nM) versus presence ([ATP] $\geq$ 92.7 nM) of ATc indicated that cellular ATP levels were significantly decreased when aldolase expression was repressed. We tested a subset of aldolase mutants that were used to complement the cKO line, again based on the different functional classes defined above.

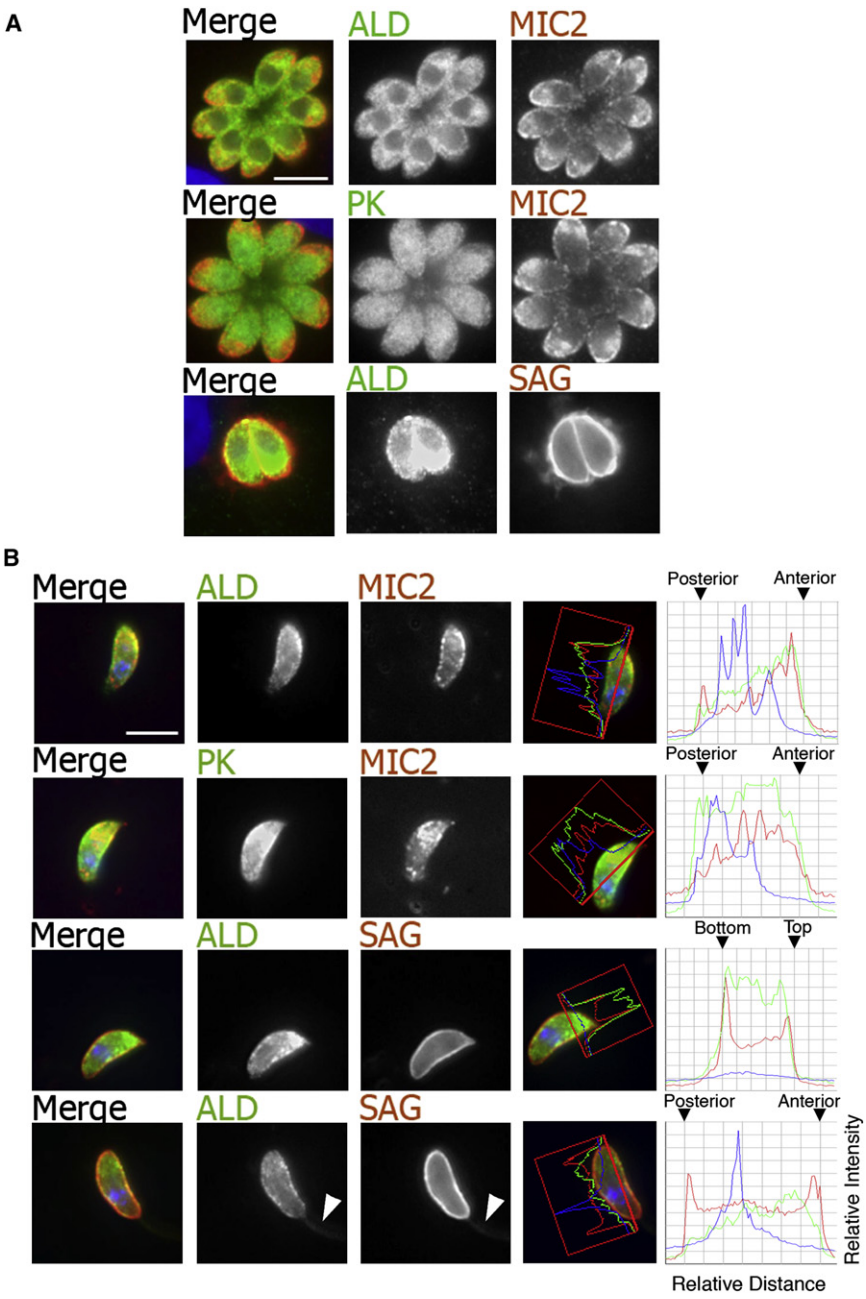

Figure 2. Localization of Aldolase during Intracellular Growth and in Extracellular Parasites Undergoing Gliding Motility

(A) Aldolase localization during intracellular growth by IF. Aldolase was detected with rabbit anti-*T. gondii* aldolase (ALD) (green) and counterstained with mouse anti-SAG1 (bottom panel, red) or rat anti-MIC2 (middle two panels, red). PK was detected with rabbit polyclonal antisera (green).

(B) IF localization of aldolase and PK in extracellular parasites during gliding motility. Selective profiles are shown to the right as histograms (color code matches the stained proteins). Staining is similar to (A). Images were deconvolved using the nearest neighbor algorithm, and a representative Z stack slice is shown. Scale bars = 5 μm.

Validation of the Aldolase-Bridging Model In Vivo

We next sought to determine if aldolase serves a critical role in bridging MIC2-actin cytoskeletal interactions during parasite motility. Following growth for 48 hr in ATc, parasites were allowed to glide on BSA-coated coverslips, and motility was evaluated as the number of trails deposited per area. In the cKO, the downregulation of aldolase resulted in a significant decrease in the number of trails produced (Figure 5C, $p \leq 0.001$). Complementation with the wild-type enzyme rescued the phenotype, while the enzyme dead mutants failed to restore normal gliding (Figure 5C). When complemented with mutants that displayed decreased binding to the MIC2t but retained enzyme activity (i.e. ALD-K41A, ALD-R42A, and ALD-K41E, R42G), motility was normal. Collectively, these results imply that the primary contribution of aldolase to parasite gliding motility is due to its role in energy production, although other explanations are also possible (see below).

Additionally, we utilized the complemented aldolase mutants to determine the contribution of aldolase to host cell invasion. Following growth in ATc, the cKO alone and clones complemented with enzyme dead mutants (i.e., ALD- D34A and ALD-R148A) exhibited a significant decrease in host cell attachment and invasion ($p \leq 0.001$) compared to complements expressing wild-type enzyme (Figure 5D). This is consistent with the lower levels of ATP generated by these mutants (Table 1) and likely indicates an energy requirement for efficient invasion. While we have not tested the K146A mutant in these assays, we would expect it to behave similarly to R148A, given their similarly compromised enzyme activity observed in vitro (Table 1). Single point mutants with normal enzyme activity but impaired binding to the MIC2t (i.e. ALD-K41A and ALD-R42A) showed normal host

The mutants that retained enzyme activity and restored parasite growth in vivo (i.e., ALD-K41A and ALD-R42A) produced equivalent if not greater levels of ATP to the wild-type complemented line (see above) (Table 1). Normal levels of ATP were also produced by the double mutant ALD-K41E, R42G, despite its lower efficiency in vitro (Table 1). Consistent with the growth assay, the enzyme null mutants (i.e. ALD-D33A and ALD-R148A) produced significantly less ATP ([ATP] $\leq$ 135, $p \leq 0.005$) than wild-type levels. These results indicate that the enzymatic activity of aldolase is crucial for ATP generation and normal parasite growth. Additionally, these results demonstrate that the defect of the double mutant ALD-K41E, R42G in the monolayer lysis assay was not due to defective ATP production.

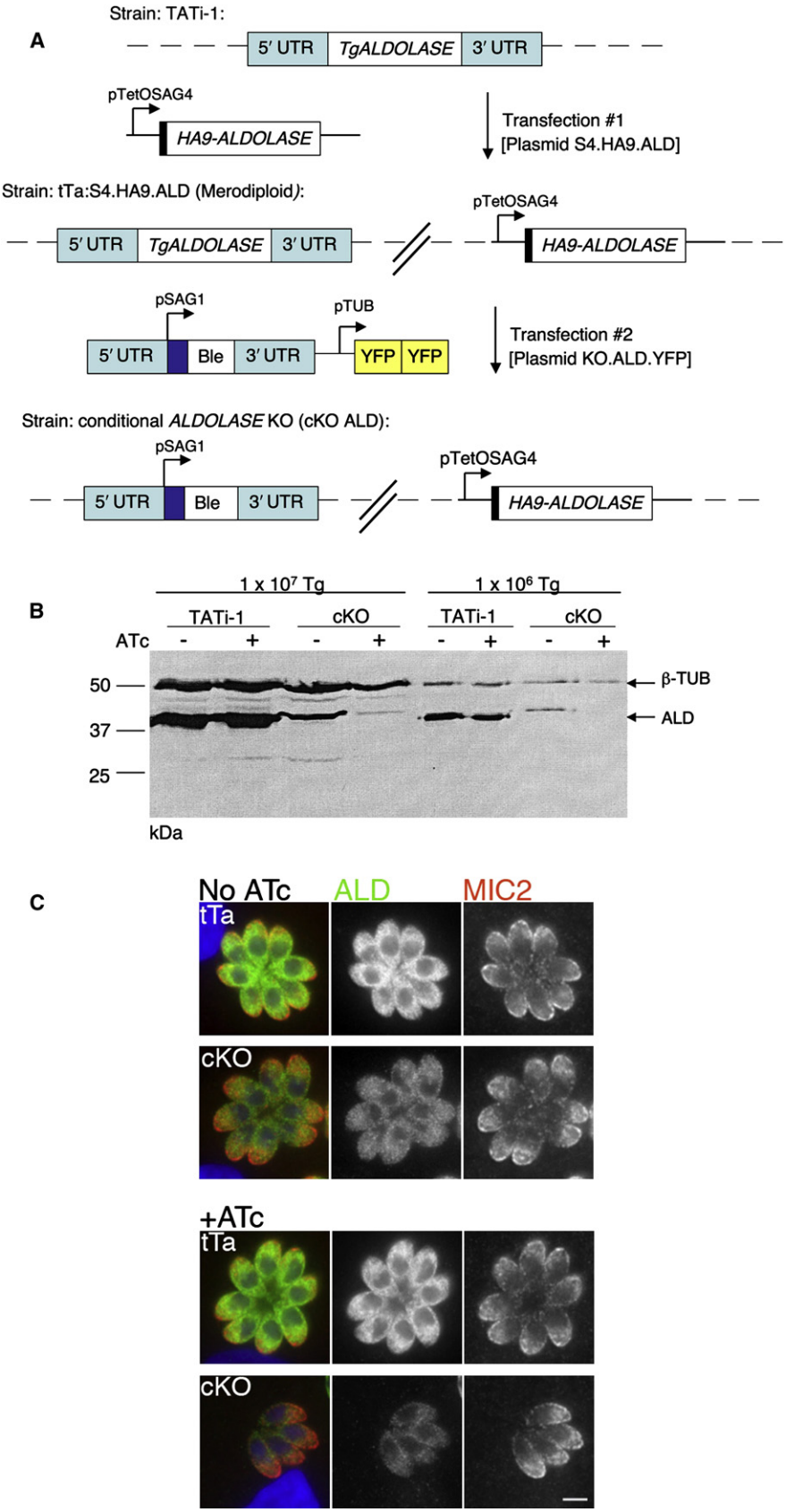
A
Strain: TATi-1:
5′ UTR
TgALDOLASE
3′ UTR
pTetOSAG4
HA9-ALDOLASE
Transfection #1
[Plasmid S4.HA9.ALD]
Strain: tTa:S4.HA9.ALD (Merodiploid):
pSAG1
pTUB
Ble
YFP
Transfection #2
[Plasmid KO.ALD.YFP]
Strain: conditional ALDOLASE KO (cKO ALD):
B
1 x 10⁷ Tg
1 x 10⁶ Tg
TATi-1
cKO
ATc
50
37
25
β-TUB
ALD
kDa
C
No ATc
ALD
MIC2
tTa
cKO
+ATc

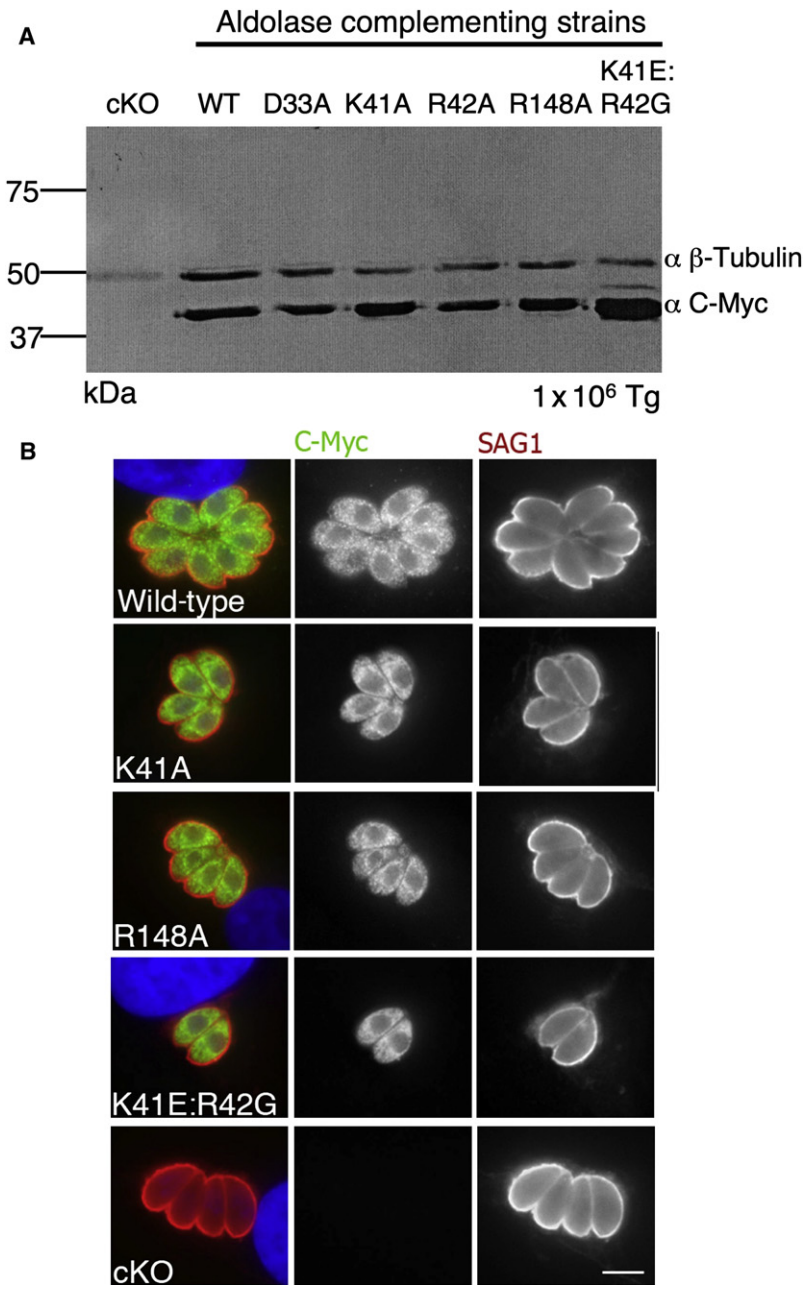

Figure 4. Expression and Localization of Aldolase Complementation Mutants

(A) Complementation of aldolase clones in the cKO background, cultured in ATc for 48 hr in 1.5 μg/ml ATc as determined by western blotting, with anti-c-Myc and rabbit anti-β-tubulin as a loading control.

(B) Localization of complementing aldolase clones by IF using an anti-c-Myc antibody (green) and SAG1 detected with DG52 (red). Images were deconvolved using the nearest neighbor algorithm; representative Z stack is shown. Scale bar = 5 μm.

cell attachment but were significantly less efficient at host cell invasion ($p \leq 0.05$, compared to the wild-type complement) (Figure 5D). The double mutant ALD-K41E, R42G also showed normal adherence to the host cell but demonstrated a far greater host cell invasion defect ($p \leq 0.005$) (Figure 5D). To more directly compare the different lines, the capacity to invade host cells following attachment was expressed as percentage total cell-associated parasites. Single mutants with impaired binding to the MIC2t showed partial reduction in the efficiency of invasion (Figure 5D). The invasive efficiency of the cKO complemented with the double mutant ALD-K41E, R42G was reduced to 41.0%, which was substantially lower than either of the enzyme dead mutants or the wild-type cKO cultured in the presence of ATc (Figure 5D). Collectively, these data indicate that aldolase enzyme activity is necessary for efficient cell invasion, in part due to a requirement for ATP, but also due to a critical role in bridging interactions between the MIC2t and the actin cytoskeleton, as shown by the mutant ALD-K41E, R42G.

DISCUSSION

We generated a cKO of *T. gondii* aldolase (*TgALD1*) to address the role of this glycolytic enzyme in bridging the cytoplasmic domain of MIC2 to the cytoskeleton in vivo. Structural modeling and point mutagenesis were used to delineate mutations that separately affected enzyme activity versus bridging of MIC2t to F-actin. Homology modeling highlighted residues in aldolase that form a basic groove and participate in electrostatic interactions with acidic residues in the MIC2t. Mutational analysis revealed that many of the charged residues in aldolase that contribute to the MIC2t interaction were also required for enzymatic activity; however, the two activities were separated into distinct subdomains, enabling independent testing of these two functions. Complementation of the aldolase cKO with various point mutants demonstrated that aldolase

Figure 3. Construction and Characterization of a Conditional Knockout of *T. gondii* Aldolase

(A) Schematic illustration of the *T. gondii* aldolase cKO. Strain TATi-1 was transfected with the regulatable, HA9-tagged TgALD1 plasmid (pS4.HA9.ALD) to establish the merodiploid parasite line (middle panel). A single merodiploid clone was transfected with the knockout plasmid (pKO.ALD.YFP) and sorted by FACS to isolate a YFP-negative cKO (bottom).

(B) Western blot analysis of TgALD1 repression following growth for 48 hr in 1.5 μg/ml ATc; probed with rabbit anti-TgALD1 and rabbit anti-β-tubulin as a loading control.

(C) IF analysis of TgALD1 repression following 24 hr in the presence of 1.5 μg/ml ATc. Aldolase (ALD) was detected using rabbit anti-*T. gondii* aldolase (green) and rat anti-MIC2 (red). Scale bar = 5 μm.

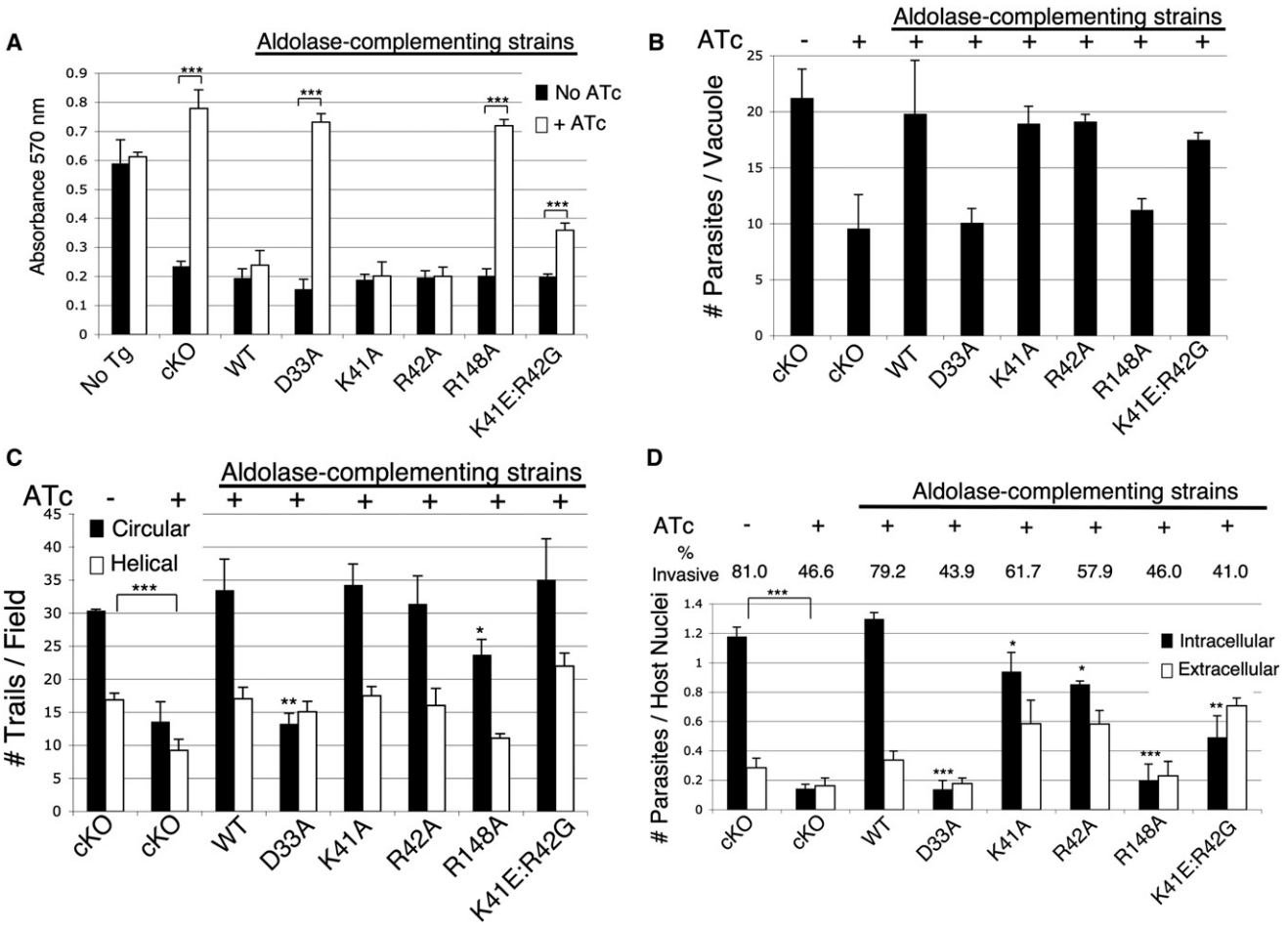

Figure 5. Complementation of the TgALD1 cKO with Biochemically Characterized Aldolase Mutants

(A) Growth of the cKO and complementing aldolase lines as monitored by monolayer lysis. Parasites were grown for 48 hr ± 1.5 μg/ml ATc prior to determination of monolayer disruption as monitored by crystal violet staining and absorbance at 570 nm. Values are means ± SD (n = 4 wells per sample from a representative experiment).

(B) Analysis of parasite growth based on average number of parasites per vacuole following 36 hr culture ± 1.5 μg/ml ATc. Values are means ± SD (n = 3 coverslips per parasite line from a representative of duplicate experiments). *$p \leq 0.05$, **$p \leq 0.005$, ***$p \leq 0.001$.

(C) Gliding motility of the cKO and aldolase-complemented lines. Values are means ± SEM for three independent experiments.

(D) Host cell invasion was evaluated using a two-color IF assay. The percent of intracellular (% invasive) parasites was determined as a function of the total number of cell-associated parasites. Mean ± SEM for three independent experiments. For (C) and (D), parasites were cultured ± 1.5 μg/ml ATc for 48 hr prior to evaluation.

contributes to parasite growth and efficient host cell invasion. A requirement for ATP generation affected motility, invasion, and growth while independent of glycolytic activity, the binding of aldolase to MIC2t was essential for efficient invasion of host cells. This requirement was shown most convincingly by the double mutant ALD-K41E, R42G, which retained normal ATP levels, replicated normally, and yet was significantly impaired in cell invasion. Collectively, these findings demonstrate an essential role in vivo for aldolase to serve as a bridge between adhesins and the cytoskeleton.

Prior mutational studies have shown the penultimate tryptophan in the cytoplasmic tails of MIC2 and TRAP contributes to the interaction with aldolase in vitro and is essential in vivo (Buscaglia et al., 2003; Jewett and Sibley, 2003; Starnes et al., 2006). Our modeling studies revealed that the indole ring of MIC2-W767 was stably anchored between the ALD-R42 and ALD-R303 side chains. However, this was not due to a cation-π interaction, which usually predominates between aromatic residues and arginine side chains during protein-protein interactions (Ma and Dougherty, 1997). Instead, the association was hydrophobic in nature, as the indole ring is stabilized by interactions with the alkyl carbons in the arginine side chains. A similar interaction was observed in cocrystal structures between rabbit muscle aldolase and a Wiskott-Aldrich Syndrome protein (WASp) peptide (St-Jean et al., 2007), as well as in a TRAPt peptide and *Plasmodium* aldolase (Bosch et al., 2007). Collectively, these studies reveal that the aldolase binding site is conserved among these different peptides, based on shared charge and hydrophobic interactions.

Homology modeling also predicted a series of electrostatic interactions between the MIC2-D765 and basic residues within

the aldolase cleft (i.e., ALD-K41, ALD-R42, and ALD-R148). Individual mutations of these charged residues partially decreased the interaction, and the double mutant ALD-K41E, R42G demonstrated a ~20-fold decrease in MIC2t binding in the pull-down assay. Interestingly, we found that the residues in aldolase that were crucial for MIC2t binding were also required for an interaction with F-actin, a subset of which were previously identified in rabbit aldolase (Wang et al., 1996). Aldolase participates in several associations unique from its role in glycolysis, including interactions with the glucose transporter GLUT-4 (Kao et al., 1999), phospholipase D (Kim et al., 2002), and the WASp peptide (St-Jean et al., 2007). The interaction with actin and MIC2t may be a case of fortuitous adaptation whereby the parasite developed a mechanism to utilize multivalent interactions to provide increased power for host cell invasion.

Previous crystallographic studies were used to predict that the residues contributing to TRAPt binding were not distinct from residues contributing to enzyme activity (Bosch et al., 2007). In contrast, our extensive mutational analysis, combined with biochemical testing, defined two residues (i.e. ALD-K41 and ALD-R42) found at the edge of the basic cleft that uniquely contributed to the MIC2t interaction. A double mutant in these residues (i.e. K41E, R42G) demonstrated an even greater decrease in binding to MIC2t. All three of these mutations maintained in vitro enzyme activity, generated normal levels of ATP, and were able to sustain normal parasite growth. The retention of normal enzyme activity in these mutants is likely attributed to the position of the ALD-K41 and ALD-R42 residues, which lie along the edge of the basic groove, jutting out at the periphery of the enzyme active site. Importantly, the role of these residues was not previously appreciated, and their identification made it possible to test the separate roles of aldolase in binding to MIC2t versus glycolysis in vivo.

The contribution of the aldolase-bridging model to parasite motility and invasion in vivo was tested using a series of aldolase mutants that were used to complement a cKO. These studies demonstrated that the predominant contribution of aldolase to parasite motility was its role in glycolysis and energy production, as all mutants that affected glycolysis also reduced motility. In contrast, mutants only affecting binding to MIC2t had no motility phenotype. This result was in contrast to what was expected and to results of a previous study examining a cKO of *TgMIC2*, in which gliding motility was impaired, and the residual gliding occurred in a nonproductive circular pattern (Huynh and Carruthers, 2006). In contrast, aldolase binding to the MIC2t and/or F-actin was required for efficient host cell invasion. The single mutants (ALD-K41A and ALD-R42A) and the double mutant ALD-K41E, R42G exhibited ~25% and 50% decreases in invasion efficiency, respectively. Decreased host cell invasion was not due to lower energy production. Hence, the phenotype of these mutants is most likely attributable to a disruption of the bridging activity required for linking the adhesin to the cytoskeleton in vivo. Collectively, these experiments suggest that MIC2t linkage to the cytoskeleton by aldolase plays a greater role when the parasite encounters resistance and traction is required (i.e. cell invasion), but may be less crucial during gliding under the in vitro conditions tested here. In the context of an in vivo infection, movement across and through tissues may require additional traction that cannot be appreciated using in vitro assays. Hence, tissue migration may have a greater reliance on aldolase for bridging. Testing this hypothesis would require an in vivo model of infection, but unfortunately, serial culture passages have completely attenuated the TATi-1 line used here for the cKO, making this experiment unfeasible.

Our findings and previous studies indicate the same region of aldolase mediates binding of substrate, actin, and the cytoplasmic tails of apicomplexan adhesins (Bosch et al., 2007; St-Jean et al., 2007; Wang et al., 1996). While F-actin and MIC2t binding are mutually exclusive within a single monomer, they may interact with different subunits in a tetramer to form a productive complex. The aldolase tetramer forms two planar dimers that are offset on the horizontal axis, positioning each dimer to interact separately. Thus, a single aldolase tetramer may present one dimer for MIC2t binding, leaving the remaining dimer for F-actin binding. Such a conformation could also potentially stabilize the filamentous state of *T. gondii* actin, which is inherently unstable (Sahoo et al., 2006).

In addition to being important for bridging to MIC2t, aldolase provides an essential function in glycolysis. Repression of the wild-type enzyme in the cKO revealed a substantial defect in cell motility and cell invasion. This likely reflects the combined effects of reduced cellular ATP and disruption in binding to the MIC2t. It has recently been reported that aldolase and other glycolytic enzymes redistribute to the inner surface of the inner membrane complex (IMC) in extracellular parasites (Pomel et al., 2008). While the role of this relocalization has not been clearly established, it was suggested that it might locally enhance energy production and hence facilitate motility. While we did not observe this peripheral localization of aldolase in extracellular parasites, the role of aldolase in glycolysis is not at odds with our findings that aldolase participates in bridging to the adhesin MIC2t. Rather, aldolase that is engaged with the tail of MIC2 is presumably partitioned between the plasma membrane and outer leaflet of the IMC and hence is segregated from the pool of aldolase in the cytosol that likely participates in glycolysis.

The binding residues that mediate the interaction of aldolase with MIC2t partially overlap with enzyme activity, and yet our data indicate that both functions are separately required for parasite survival. This raises important questions about how the parasite is capable of coordinating these two mutually exclusive functions under conditions where they might coexist in the cell. Given the estimated binding affinity in physiologic salt ($K_D \sim 0.375$ μM [G.L.S. and L.D.S., unpublished data]) and relative stoichiometry (3 μM MIC2 versus 30 μM TgALD1 [G.L.S. and L.D.S., unpublished data]), the majority of the MIC2t is predicted to be complexed with aldolase in the cytoplasm without significantly decreasing the amount of enzyme available for glycolysis (i.e., in the absence of substrate, the predicted MIC2t occupancy is ~98%, leaving 90% of aldolase free). While not a direct measure of interaction affinities, the results from the purified protein pull-down assay can be used to estimate the amount of MIC2t that is occupied in the cKO complemented with various mutants. For example, in the ALD-K41E, R42G double mutant, the interaction is decreased 20-fold, but the cellular concentration of MIC2 does not change, and thus 30% of the cellular stores of MIC2 will likely be occupied by aldolase as a result. This level

of occupancy may explain the residual invasion seen with the double mutant. The residual invasion and motility phenotypes of the single and double mutants may also be due to incomplete shutdown by ATc and the resulting residual activity of wild-type aldolase (estimated to be ~5%). As a consequence, partial occupancy of MIC2-ALD may be sufficient to transiently engage the cytoskeleton and mask any potential role of aldolase in motility. Additionally, our previous studies demonstrated that a second, upstream cluster of acidic residues in the MIC2t is also essential in vivo, yet does not participate in aldolase binding (Starnes et al., 2006). Hence, it remains possible that other proteins contribute to linking MIC2 and possibly related adhesins to the cytoskeleton. Despite these limitations, our studies clearly define an important role for aldolase binding to MIC2t in facilitating efficient parasite invasion. In the absence of this bridging activity, parasite invasion was significantly decreased despite maintaining normal levels of ATP.

Our studies reveal that aldolase not only impacts energy production but also stabilizes interactions between adhesins and the actin cytoskeleton, thereby increasing the efficiency of invasion. Detailed biochemical and mutational analyses delineated specific residues critical for linking the cytoplasmic tail of MIC2 to the cytoskeleton and separated this function from residues participating in cellular energy production. In vivo complementation of the cKO further elucidated the requirement of aldolase bridging in apicomplexan host cell invasion. Our findings demonstrate that aldolase functions in a complex to bridge MIC2 to the cytoskeleton in vivo. Disruption of this interaction, combined with inhibition of other key components in the motor complex, may allow new avenues of treatment to prevent infection by apicomplexan parasites.

EXPERIMENTAL PROCEDURES

Growth of Host Cells and Parasite Strains

T. gondii tachyzoites were maintained by growth in monolayers of human foreskin fibroblasts (HFFs) cultured in complete medium and supplemented tetracycline-free fetal bovine serum (HyClone; Logan, UT) (Starnes et al., 2006). Chloramphenicol (20 μg/ml) (Sigma-Aldrich), phleomycin (5 μg/ml) (InvivoGen), ATc (1.5 μg/ml) (Clontech; Palo Alto, CA), and pyrimethamine (3 μM) (Sigma-Aldrich) were added to the media as indicated.

Aldolase: GST-MIC2t Fusion Protein Pull-Down Assays

GST-MIC2t (containing residues 721–769 of MIC2) was purified from the *E. coli* BL21 strain and used for pull-down assays, as described previously (Starnes et al., 2006). Recombinant *T. gondii* aldolase was coincubated with GST-MIC2t or GST alone, and bound proteins were eluted in sample buffer, resolved by SDS-PAGE, stained with SYPRO Ruby Protein Gel Stain (Molecular Probes; Eugene, OR), and quantified using a FLA-5000 phosphorimager (Fuji Film Medical Systems; Stamford, CT).

Cosedimentation Assay

Purified rabbit skeletal muscle actin (Cytoskeleton, Inc.; Denver) was diluted to 10 μM in 1× G-Buffer (5 mM Tris [pH 8.0], 0.2 mM $CaCl_2$, 0.5 mM DTT, 0.2 mM ATP) and centrifuged at 100,000× *g* for 45 min using a TL100 rotor in a Beckman Optima TL Ultracentrifuge (Beckman Coulter; Fullerton, CA). Actin was polymerized by the addition of 1/10 total volume 10× F-Buffer (500 mM KCl, 20 mM $MgCl_2$, 10 mM ATP) at room temperature for 1 hr. Purified aldolase was added to polymerized actin in a 1:10 molar ratio, allowed to bind for 30 min at room temperature, and centrifuged at 100,000× *g* for 1 hr at 25°C. The pellet was resuspended in sample buffer, resolved by 10% SDS-PAGE and aldolase detected by western blot analysis, and quantified using an FLA-5000 phosphorimager.

Determination of Enzyme Activity

In vitro aldolase activity was determined by measuring NADH oxidation as a function of decreasing absorption/minute at 340 nm (St-Jean et al., 2005). Assays were performed in triplicate using a Beckman Coulter DU-640 Spectrophotometer and K_M and V_{max} values determined using the Michaelis-Menten equation in the KaleidaGraph 4.0 (Synergy Software; Reading, PA).

Antibodies

Aldolase was detected using rabbit polyclonal antisera to TgALD1 (Starnes et al., 2006). MIC2 was detected using rat polyclonal sera to the MIC2 ectodomain. *T. gondii* β-tubulin was detected using rabbit polyclonal antisera (Morrissette and Sibley, 2002). The surface antigen, SAG1, was detected with the monoclonal antibody DG52. PK was detected using rabbit polyclonal antisera, generously contributed by Takashi Asai (Keio University, Tokyo). c-Myc was detected with monoclonal antibody 9E10 (Invitrogen; Carlsbad, CA).

Immunofluorescence Microscopy

For immunofluorescence (IF), localization-infected monolayers of HFF cells or freshly egressed parasites were fixed with 4% formaldehyde in PBS for 20 min at 4°C and permeabilized with 0.25% Triton X-100 or 0.1% saponin, as described previously (Starnes et al., 2006). Images were acquired in wide field as Z stack series (0.25 μm steps) using a Zeiss Axioskop 2 MOT Plus microscope equipped with a 63× 1.3 numerical aperture lens and a AxioCam MRm camera (Carl Zeiss, Inc.; Thornwood, NY). Images were deconvolved using the nearest neighbor algorithm, and profiles were generated from representative Z slices in AxioVision v4.2.

Generation of Aldolase Expression and Knockout Constructs

Amino-terminal HIS_6-tagged *TgALD1* was generated by PCR amplification (Jewett and Sibley, 2003) and directionally cloned into the pET16b vector (Novagen; Madison, WI) using the NdeI and BamHI restriction sites. The aldolase point mutants were generated using the QuikChange Site-Directed Mutagenesis Kit from Stratagene (Cedar Creek, TX). Proteins were induced in BL21 *E. coli* and purified using nickel affinity chromatography, and purity was checked by SDS-PAGE.

To generate constructs for regulated expression, N-terminally HA9-tagged *TgALD1* was PCR amplified and cloned into the regulated expression vector p7TetOS4 (Meissner et al., 2002) using the restriction sites EcoRI and PacI to generate the plasmid pS4.HA9.ALD. To provide selection, the *CAT* gene driven by the *SAG1* promoter (Kim et al., 1993) was cloned into the SacII site in pS4.HA9.ALD.

To generate plasmids for creating a genomic knockout of aldolase, the Ble selectable marker conferring phleomycin resistance (Messina et al., 1995) was flanked by 2 kb of upstream and downstream genomic sequence of TgALD1 (46.m00002; http://www.toxo.db.org). To provide negative selection, a tandem YFP cassette driven by the α-tubulin promoter (kindly provided by Boris Striepen) was inserted at the SacI restriction site to generate the plasmid pKOAld:YFP.

To complement the aldolase cKO strain, a plasmid expressing N-terminally c-Myc-tagged aldolase was generated by replacing the *Ble* gene in the vector SAG1/Ble/SAG1 (Messina et al., 1995) with wild-type *TgALD1*. The DHFR selectable marker, conferring resistance to pyrimethamine (Donald and Roos, 1993), was inserted to generate the plasmid pC-Myc.WTALD.DHFR.

Generation of the Aldolase cKO and Complementing Mutants

The TATi-1 line was transfected by electroporation with the plasmid pS4.HA9.ALD and stable transformants selected using chloramphenicol (Kim et al., 1993). A representative clone was transfected with linearized pKOAld:YFP plasmid selected with phleomycin (Messina et al., 1995), followed by sorting to recover YFP-negative clones using a Dako MoFlo (Carpinteria, CA). A representative cKO clone was transfected with wild-type or mutant aldolase genes to establish stable transgenic lines. Clones were selected with 3 μM pyrimethamine, and expression was confirmed by staining for the c-Myc epitope.

Growth Assays

Growth was monitored using a monolayer lysis assay, as described previously (Brossier et al., 2008). Following growth in the absence or presence of ATc

(1.5 μg/ml), monolayers were fixed with 70% EtOH and stained with 0.1% crystal violet, and absorbance was read at 570 nm using the EL800 multiwell plate reader (BioTek Instruments, Inc.; Winooski, VT), in three independent experiments.

Parasite growth was determined by counting the number of parasites per vacuole at 36 hr postinfection, as described previously (Taylor et al., 2006). Parasites were harvested and used to infect HFF cells grown on glass coverslips. After culture at 37°C 5% CO_2 for 36 hr (±ATc), monolayers were fixed for IF, stained for the surface antigen SAG1 using mAb DG52, and mounted with Vectashield containing DAPI. Coverslips were examined by epifluorescence microscopy, and the average number of parasites per vacuole was determined from 30 randomly selected vacuoles per coverslip (n = 3) in three independent experiments.

Determination of Cellular ATP

Cellular concentrations of ATP were determined using the CellTiter-Glo Luminescent Cell Viability Assay (Promega; Madison, WI) according to manufacturer's protocol, and luminescence was determined using a BioTek Synergy 2 Multi-Mode Microplate Reader coordinated with Gen5 reader control and data analysis software. Selective transgenes expressed in the cKO were grown in the presence of ATc for 48 hr, harvested when they egressed, and tested in triplicate.

Gliding Assay

Parasites were grown for 48 hr in the presence or absence of 1.5 μg/ml ATc. Freshly harvested parasites were allowed to glide on BSA-coated coverslips for 25 min at 37°C, fixed for IF, and stained with antisera to the surface antigen SAG1 to detect trails, as described previously (Brossier et al., 2008). The total number of trails (circular and helical) per field for five fields per coverslip (n = 3) were determined in triplicate in three independent experiments.

Invasion Assay

Invasion of HFF cells cultured on coverslips was performed using a two-color IF staining protocol to distinguish extracellular from intracellular parasites, as previously described (Brossier et al., 2008). Intracellular and extracellular parasites were determined by microscopic examination of five fields per coverslip (n = 3) and expressed as function of total host cells per field.

Generation of Homology Models

The structure of fructose-bisphosphate aldolase from *Plasmodium falciparum* in complex with the TRAP-tail (PDB entry: 2PC4) was used to build a homology model of *T. gondii* aldolase. A subunit of the muscle aldolase tetramer was modeled with the *T. gondii* aldolase sequence using Modeler software (Eswar et al., 2007) based on ten trial models. The model with lowest energy and best MolProbity score (Lovell et al., 2003) was retained for modeling the TgALD1-MIC2 interaction.

The MIC2 tail sequence in *T. gondii* aldolase was threaded according to the WASp conformation obtained in the structure of rabbit muscle aldolase in complex with a C-terminal peptide of WASp (PDB entry: 2OT0) after superposition of the two aldolase structures. The resultant model was minimized with GROMACS (Berendsen et al., 1995) package using the all-atom force field GROMOS96 (parameter set 43a1). Minimization consisted of 600 steps of steepest descent followed by 1000 cycles of conjugate gradient minimization. A 2 ns molecular dynamic simulation was then run using the position-restrained option in GROMACS to optimize fit of the MIC2 peptide in the *T. gondii* aldolase-binding site. The final model geometry was checked by MolProbity, which generated a score of 2.05.

SUPPLEMENTAL DATA

Supplemental Data include Supplemental References, two tables, and one figure and can be found online at http://www.cell.com/cell-host-microbe/supplemental/S1931-3128(09)00096-1.

ACKNOWLEDGMENTS

We thank J.P. Vogel and S. Lourido for thoughtful discussions and comments; J. Nawas and J. LaFrance-Vanasse for technical assistance; and B. Eades, Siteman Cancer Center, for assistance with cell sorting. This work was funded by NIH grant AI034036 (to L.D.S.), with partial support from institutional training grant AI07172-26 (to G.L.S.) and a grant from the Natural Science and Engineering Research Council of Canada (to J.S.).

Received: October 24, 2008
Revised: January 20, 2009
Accepted: March 13, 2009
Published: April 22, 2009

REFERENCES

Berendsen, H.J.C., van der Spoel, D., and van Drunen, R. (1995). Gromacs: a message-passing parallel molecular dynamics implementation. Comput. Phys. Commun. *91*, 43–56.

Bosch, J., Buscaglia, C.A., Krumm, B., Ingason, B.P., Lucas, R., Roach, C., Cardozo, T., Nussenzweig, V., and Hol, W.G. (2007). Aldolase provides an unusual binding site for thrombospondin-related anonymous protein in the invasion machinery of the malaria parasite. Proc. Natl. Acad. Sci. USA *104*, 7015–7020.

Brossier, F., Starnes, G.L., Beatty, W.L., and Sibley, L.D. (2008). Microneme rhomboid protease TgROM1 is required for efficient intracellular growth of Toxoplasma gondii. Eukaryot. Cell *7*, 664–674.

Buscaglia, C.A., Coppens, I., Hol, W.G.J., and Nussenzweig, V. (2003). Site of interaction between aldolase and thrombospondin-related anonymous protein in Plasmodium. Mol. Biol. Cell *14*, 4947–4957.

Dessens, J.T., Beetsma, A., Dimopoulos, G., Wengelnik, K., Crisanti, A., Kafatos, F.C., and Sinden, R.E. (1999). CTRP is essential for mosquito infection by malaria ookinetes. EMBO J. *18*, 6221–6227.

Dobrowolski, J.M., and Sibley, L.D. (1996). Toxoplasma invasion of mammalian cells is powered by the actin cytoskeleton of the parasite. Cell *84*, 933–939.

Donald, R.G.K., and Roos, D.S. (1993). Stable molecular transformation of Toxoplasma gondii: A selectable dihydrofolate reductase-thymidylate synthase marker based on drug resistance mutations in malaria. Proc. Natl. Acad. Sci. USA *90*, 11703–11707.

Eswar, N., Webb, B., Marti-Renom, M.A., Madhusudhan, M.S., Eramian, D., Shen, M.Y., Pieper, U., and Sali, A. (2007). Comparative protein structure modeling using MODELLER protein. Curr. Protoc. Protein Sci. *Chapter 2*, Unit 2.9.

Gaskins, E., Gilk, S., DeVore, N., Mann, T., Ward, G.E., and Beckers, C. (2004). Identification of the membrane receptor of a class XIV myosin Toxoplasma gondii. J. Cell Biol. *165*, 383–393.

Harper, J.M., Hoff, E.F., and Carruthers, V.B. (2004). Multimerization of the Toxoplasma gondii MIC2 integrin-like A domain is required for binding to heparin and human cells. Mol. Biochem. Parasitol. *134*, 201–212.

Hill, D., and Dubey, J.P. (2002). Toxoplasma gondii transmission, diagnosis and prevention. Clin. Microbiol. Infect. *8*, 634–640.

Huynh, M.H., and Carruthers, V.B. (2006). Toxoplasma MIC2 is a major determinant of invasion and virulence. PLoS Pathog. *2*, 753–762.

Jewett, T.J., and Sibley, L.D. (2003). Aldolase forms a bridge between cell surface adhesins and the actin cytoskeleton in apicomplexan parasites. Mol. Cell *11*, 885–894.

Kao, A.W., Noda, Y., Johnson, J.H., Pessin, J.E., and Saltiel, A.R. (1999). Aldolase mediates the association of F-actin with the insulin-responsive glucose transporter GLUT4. J. Biol. Chem. *274*, 17742–17747.

Kim, J.H., Lee, S., Lee, T.G., Hirata, M., Suh, P.F., and Ryu, S.H. (2002). Phospholipase D2 directly interacts with aldolase via its PH domain. Biochemistry *41*, 3414–3421.

Kim, K., Soldati, D., and Boothroyd, J.C. (1993). Gene replacement in Toxoplasma gondii with chloramphenicol acetyltransferase as selectable marker. Science *262*, 911–914.

Lovell, S.C., Davis, I.W., Arendall, W.B., 3rd, de Bakker, P.I., Word, J.M., Prisant, M.G., Richardson, J.S., and Richardson, D.C. (2003). Structure validation by Calpha geometry: phi, psi and Cbeta deviation. Proteins *50*, 437–450.

Ma, J.C., and Dougherty, D.A. (1997). The cation-pi interaction. Chem. Rev. *97*, 1303–1324.

Meissner, M., Schluter, D., and Soldati, D. (2002). Role of Toxoplasma gondii myosin A in powering parasite gliding and host cell invasion. Science *298*, 837–840.

Ménard, R. (2001). Gliding motility and cell invasion by Apicomplexa: insights from the Plasmodium sporozoite. Cell Microbiol. *3*, 63–73.

Messina, M., Niesman, I.R., Mercier, C., and Sibley, L.D. (1995). Stable DNA transformation of Toxoplasma gondii using phleomycin selection. Gene *165*, 213–217.

Meyerhof, O., Lohmann, K., and Schuster, P.H. (1936). Uber die Aldose, ein Kohlenstoff-verknüpfendes ferment. Biochem. Z. *286*, 301–319.

Morrissette, N.S., and Sibley, L.D. (2002). Disruption of microtubules uncouples budding and nuclear division in Toxoplasma gondii. J. Cell Sci. *115*, 1017–1025.

Opitz, C., and Soldati, D. (2002). "The glideosome": a dynamic complex powering gliding motion and host cell invasion by Toxoplasma gondii. Mol. Microbiol. *45*, 597–604.

Penhoet, E., Kochman, M., Valentine, R., and Rutter, W.J. (1967). The subunit structure of mammalian fructose diphosphate aldolase. Biochemistry *6*, 2940–2949.

Pomel, S., Luk, F.C.Y., and Beckers, C.J.M. (2008). Host cell egress and invasion induce marked relocations of glycolytic enzymes in Toxoplasma gondii tachyzoites. PLoS Pathog. *4*, e1000188.

Robson, K.J.H., Frevert, U., Reckmann, I., Cowan, G., Beier, J., Scragg, I.G., Takehara, K., Bishop, D.H.L., Pradel, G., Sinden, R., et al. (1995). Thrombospondin-related adhesive protein (TRAP) of Plasmodium falciparum: expression during sporozoite ontogeny and binding to human hepatocytes. EMBO J. *14*, 3883–3894.

Sahoo, N., Beatty, W.L., Heuser, J.E., Sept, D., and Sibley, L.D. (2006). Unusual kinetic and structural properties control rapid assembly and turnover of actin in the parasite Toxoplasma gondii. Mol. Biol. Cell *17*, 895–906.

Sibley, L.D. (2004). Invasion strategies of intracellular parasites. Science *304*, 248–253.

Spano, F., Putignani, L., Naitza, S., Puri, C., Wright, S., and Crisanti, A. (1998). Molecular cloning and expression analysis of a Cryptosporidium parvum gene encoding a new member of the thrombospondin family. Mol. Biochem. Parasitol. *92*, 147–162.

St-Jean, M., LaFrance-Vanasse, J., Liotard, B., and Sygusch, J. (2005). High resolution reaction intermediates of rabbit muscle fructose-1,6-bisphosphate aldolase: substrate cleavage and induced fit. J. Biol. Chem. *280*, 27262–27270.

St-Jean, M., Izard, T., and Sygusch, J. (2007). A hydrophobic pocket in the active site of glycolytic aldolase mediates interactions with Wiskott-Aldrich syndrome protein. J. Biol. Chem. *282*, 14309–14315.

Starnes, G.L., Jewett, T.J., Carruthers, V.B., and Sibley, L.D. (2006). Two separate, conserved acidic amino acid domains within the Toxoplasma gondii MIC2 cytoplasmic tail are required for parasite survival. J. Biol. Chem. *281*, 30745–30754.

Sultan, A.A., Thathy, V., Frevert, U., Robson, K.J.H., Crisanti, A., Nussenzweig, V., Nussenzweig, R.S., and Menard, R. (1997). TRAP is necessary for gliding motility and infectivity of Plasmodium sporozoites. Cell *90*, 511–522.

Sygusch, J., Beaudry, D., and Allaire, M. (1987). Molecular architecture of rabbit skeletal muscle aldolase at 2.7 Angstrom resolution. Proc. Natl. Acad. Sci. USA *84*, 7846–7850.

Taylor, S., Barragan, A., Su, C., Fux, B., Fentress, S.J., Tang, K., Beatty, W.L., Hajj, E.L., Jerome, M., Behnke, M.S., et al. (2006). A secreted serine-threonine kinase determines virulence in the eukaryotic pathogen Toxoplasma gondii. Science *314*, 1776–1780.

Tomley, F.M., Clarke, L.E., Kawazoe, U., Dijkema, R., and Kok, J.J. (1991). Sequence of the gene encoding an immunodominant microneme protein of Eimeria tenella. Mol. Biochem. Parasitol. *49*, 277–288.

Wan, K.L., Carruthers, V.B., Sibley, L.D., and Ajioka, J.W. (1997). Molecular characterisation of an expressed sequence tag locus of Toxoplasma gondii encoding the micronemal protein MIC2. Mol. Biochem. Parasitol. *84*, 203–214.

Wang, J., Morris, A.J., Tolan, D.R., and Pagliaro, L. (1996). The molecular nature of the F-actin binding activity of aldolase revealed with site-directed mutants. J. Biol. Chem. *271*, 6861–6865.

Wetzel, D.M., Håkansson, S., Hu, K., Roos, D.S., and Sibley, L.D. (2003). Actin filament polymerization regulates gliding motility by apicomplexan parasites. Mol. Biol. Cell *14*, 396–406.

Yuda, M., Sakaida, H., and Chinzei, Y. (1999). Targeted disruption of the Plasmodium berghei CTRP gene reveals its essential role in malaria infection of the vector mosquito. J. Exp. Med. *190*, 1711–1715.